Optical Engineering

OpticalEngineering.SPIEDigitalLibrary.org

Robust and accurate star segmentation algorithm based on morphology

Jie Jiang
Liu Lei
Zhang Guangjun

SPIE.

Jie Jiang, Liu Lei, Zhang Guangjun, "Robust and accurate star segmentation algorithm based on morphology," *Opt. Eng.* **55**(6), 063101 (2016), doi: 10.1117/1.OE.55.6.063101.

Robust and accurate star segmentation algorithm based on morphology

Jie Jiang, Liu Lei,* and Zhang Guangjun
Beihang University, Key Laboratory of Precision Opto-Mechatronics Technology, Ministry of Education, Beijing 100191, No. 37 Xueyuan Road, Haidian District, Beijing, China

Abstract. Star tracker is an important instrument of measuring a spacecraft's attitude; it measures a spacecraft's attitude by matching the stars captured by a camera and those stored in a star database, the directions of which are known. Attitude accuracy of star tracker is mainly determined by star centroiding accuracy, which is guaranteed by complete star segmentation. Current algorithms of star segmentation cannot suppress different interferences in star images and cannot segment stars completely because of these interferences. To solve this problem, a new star target segmentation algorithm is proposed on the basis of mathematical morphology. The proposed algorithm utilizes the margin structuring element to detect small targets and the opening operation to suppress noises, and a modified top-hat transform is defined to extract stars. A combination of three different structuring elements is utilized to define a new star segmentation algorithm, and the influence of three different structural elements on the star segmentation results is analyzed. Experimental results show that the proposed algorithm can suppress different interferences and segment stars completely, thus providing high star centroiding accuracy. [DOI: 10.1117/1.OE.55.6.063101]

Keywords: image processing; mathematical morphology; top-hat transform; star segmentation; star tracker.

Paper 151356 received Sep. 28, 2015; accepted for publication May 3, 2016; published online Jun. 1, 2016.

1 Introduction

A spacecraft's attitude plays an important role in celestial navigation and attitude control. Star sensors are the most widely used instrument in celestial navigation, which are based on matching stars from an obtained star image to a star catalog. A star sensor primarily includes three processes, namely, star segmentation, star pattern recognition, and attitude determination. As a critical and basic step in the design of a star sensor, star segmentation influences the accuracy and efficiency of the subsequent steps. A star image includes stars and different interferences; these interferences include single point noise, Gaussian noise, read noise, fixed pattern noise, dark current shot noise, photon shot noise, and so on, and varying illumination such as moonlight.[1,2] Stars will not be segmented accurately without removing the interference, which affects attitude accuracy. Thus, interference suppression and accurate star segmentation are major issues in star segmentation.[3–5]

Traditional star segmentation is done by global thresholding.[6–8] Global thresholding, however, is appropriate only for images with uniformly distributed intensity. Given the uneven illumination in star images with the moon, the histogram of these images is inseparable into distinct partitions. It cannot remove interferences and thus cannot extract stars accurately. Therefore, one global threshold is impractical, and a set of local thresholds based on image local characteristics is useful instead.

Mao proposed a local thresholding algorithm based on the Niblack algorithm;[9,10] it can remove uneven illumination interference, but the star segmentation is incomplete and cannot guarantee centroiding accuracy. Arbabmir also proposed a local threshold method for star image processing that is based on the Bernsen algorithm;[11] it cannot suppress noises effectively and cannot remove the interference completely.

A star is a type of small target in star images, and star segmentation can be classified as small target detection.[12–15] Top-hat transform in mathematical morphology[16–19] can be utilized in small target detection. Given the shortcomings of classical top-hat transform, Bai proposed the new top-hat transform (NWTH).[20] NWTH can enhance infrared dim small targets more efficiently than a classical top-hat transform. So far, there has been no application of mathematical morphology in star image segmentation.

In considering the advantages and disadvantages of the discussed methods, this study proposes a new star target segmentation (NSTS) algorithm based on the characteristics of stars and different interferences. The algorithm utilizes the margin structuring element to detect small targets and opening operation to suppress noises. A combination of three different structuring elements is adopted to organize a new transform.

This paper is organized as follows. Section 2 provides the definition of NSTS and the principle of star image processing. Section 3 provides an analysis of the effects of different structuring elements of star image processing results. Section 4 presents the experimental results for a set of test images and a comparison with other algorithms. Section 5 presents the conclusion.

2 New Star Target Segmentation

Mathematical morphological operations work with two sets: an original image and structuring element.[17] Flat structuring element is one the most widely used structuring elements and is easy to use. Moreover, the NSTS given in this paper is based on a flat structuring element. Let $I(x, y)$ and

*Address all correspondence to: Liu Lei, E-mail address: kobeliulei@126.com

B represent the grayscale image and structuring element. Some of the basic morphological operations we will use are

Dilation: $I\Theta B = \max_{i,j}(x+i, y+j)$
Erosion: $I \oplus B = \max_{i,j}(x-i, y-j)$
Opening: $I \circ B = I\Theta B \oplus B$

The star image contains stars and different interferences. Stars and noise are all unflat regions in the star image, but the star region size is larger than the unflat noise. Meanwhile, the margin structuring element has the capacity to detect small targets and the opening operation has the capacity to suppress noise. The definitions of opening operation and close operation indicate that the gray level of opening operation is lower than the original image, and the gray level of close operation is higher than original image. Thus, the NSTS was proposed.

Let B_{Mi} and B_{Mo} represent two flat square structuring elements. Let $D(B)$ represent the size of structuring element B, which is the length of the square structuring element. Suppose that $D(B_{Mi}) < D(B_{Mo})$ and let B_M represent the margin region between B_{Mi} and B_{Mo}. $d(B_M)$ is the width of the margin structuring element; thus, $d(B_M) = (1/2)[D(B_{Mo}) - D(B_{Mi})]$. B_E represents a flat square structuring element and $D(B_{Mo}) \geq D(B_E)$. Let B_S represent the flat structuring element, and the size of B_S should be larger than the noise and smaller than a star. The relationship among B_M, B_S, B_E, B_{Mi}, B_{Mo} is shown in Fig. 1.

Define NSTS as follows:

$$K(x,y) = I(x,y) \circ B_S, \tag{1}$$

$$N(x,y) = I(x,y) \oplus B_M \Theta B_E, \tag{2}$$

$$R(x,y) = K(x,y) - \min[K(x,y), N(x,y)]. \tag{3}$$

In these equations, $I(x,y)$ represents the original image and $K(x,y)$ represents the result of the opening operation by structuring element B_S, which has the function of suppressing noise, based on the definition of opening operation. The gray level of $K(x,y)$ is lower than thegray level of $I(x,y)$. $N(x,y)$ represents the result of the erosion operation by structuring element B_E after the dilation operation by margin structuring element B_M, namely, the new close operation, which has the function of the detecting star. $R(x,y)$ represents $K(x,y)$ subtracted by the minimum of $K(x,y)$ and $N(x,y)$, i.e., the modified top-hat transform. If the gray level of $N(x,y)$ is lower than the gray level of $K(x,y)$, a star is detected and reserved; otherwise, the interference is suppressed. Finally, if $R(x,y) > 0$, then the pixel of (x,y) in the image is considered a star pixel, so star segmentation is realized. Each step of the NSTS is shown in Fig. 2.

Given that the opening operation has the effect of suppressing noise, noise with a size smaller than the size of B_S can be removed, and the margin structuring element can be utilized to detect stars. From the properties of NWTH, a large $d(B_M)$ indicates strong noise smoothing capability. NSTS utilizes the opening operation to suppress noises. Therefore, the noise smoothing capability depends not only on the width of $d(B_M)$ but also on the opening operation. $d(B_M)$ can thus be reduced. On the basis of the relationship among B_M, B_S, B_E, B_{Mi}, B_{Mo}, $D(B_{Mo})$ and $D(B_E)$ can be decreased, which reduces the amount of calculation, and thereby reduces the computation time. The influence of the size of structuring elements will be discussed in Sec. 3.

A star image that contains moonlight interference is considered as an example in this study. The star image contains stars and interferences of noise and moonlight, as shown in Fig. 3. The gray level of the star region changes significantly, whereas the gray level of the background changes insignificantly and contains a single-point noise. The gray level of the moonlight region is relatively high.

The principle of NSTS is shown in Fig. 4. The blue line represents the gray curve of the original image $I(x,y)$, the green line represents the gray curve of the opening operation result $K(x,y)$, and the red line represents the gray curve of $N(x,y)$.

First, the structuring element B_S is used to perform the opening operation on $I(x,y)$ to obtain $K(x,y)$, as shown by the green curve in Fig. 4. After the opening operation, the unflat region and noise with small size, such as single-point noise, is smoothed. Considering that the size of B_S is smaller

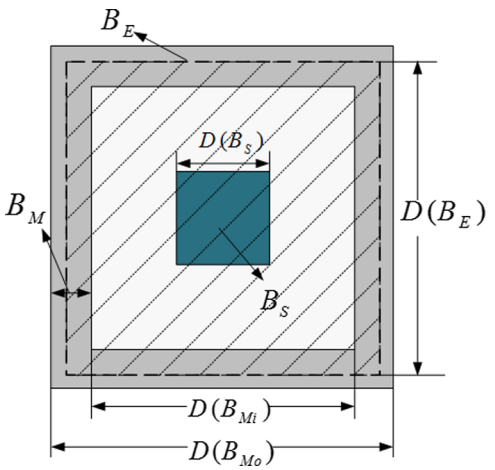

Fig. 1 Definition of structuring elements.

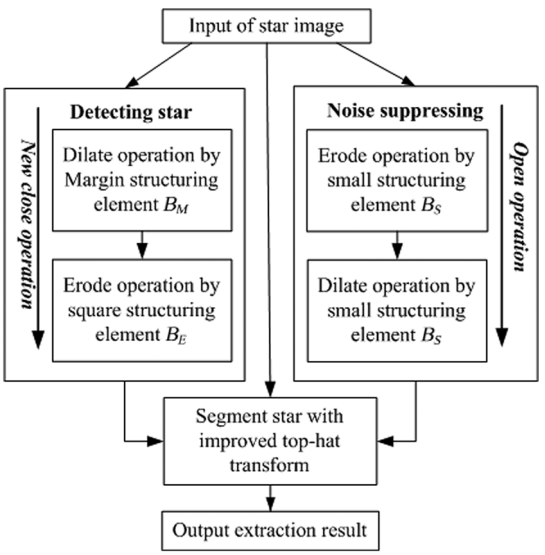

Fig. 2 Flowchart of the proposed algorithm.

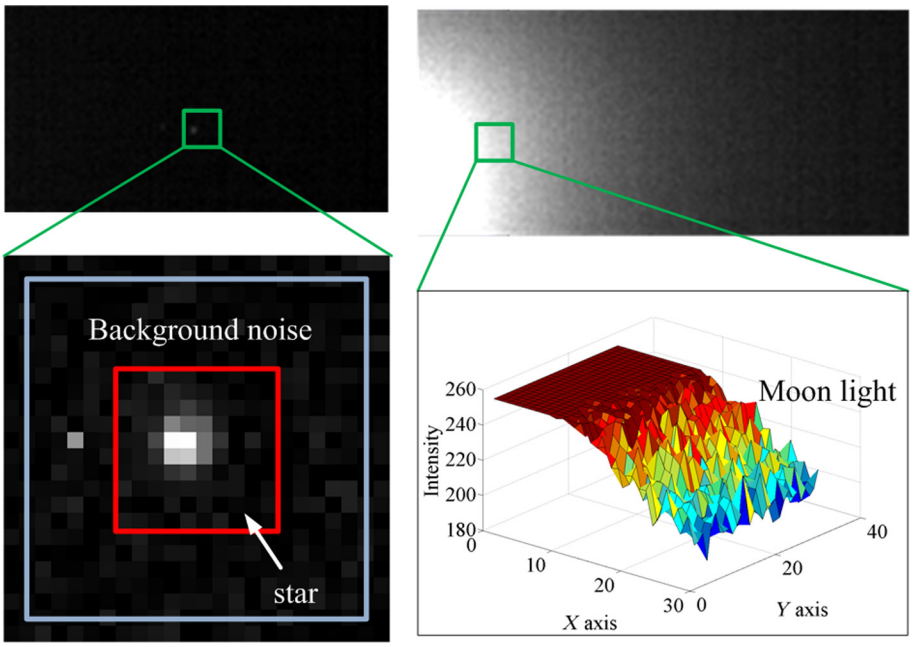

Fig. 3 Schematic of star and moonlight regions.

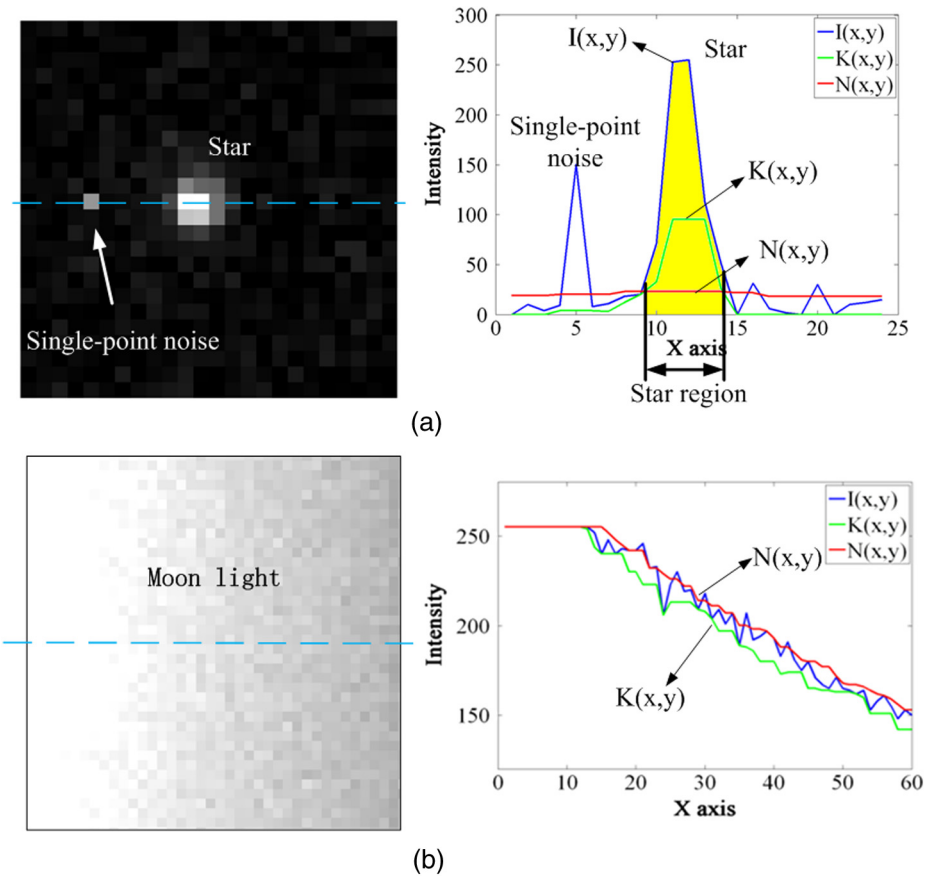

Fig. 4 Illustration of NSTS algorithm (a) process of the star region and (b) process of the moonlight region.

than the size of the star, the opening operation cannot remove the star. According to the characteristics of the opening operation, $K(x,y) \leq I(x,y)$ exists.

Second, $N(x,y)$ represents the erosion operation by structuring element B_E after the dilation operation by margin structuring element B_M, as shown by the red curve in Fig. 4. In the star region, $N(x,y)$ is the gray level of background noise. Given that the gray level of in the star region is larger than the gray level of background noise, $N(x,y) < I(x,y)$, the star region is detected; in the region

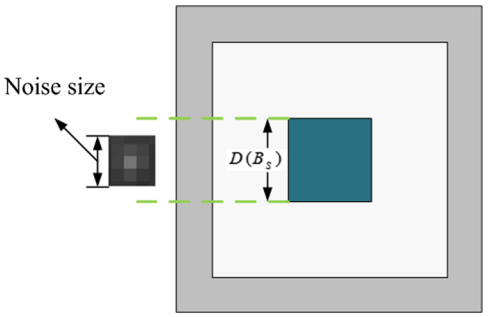

Fig. 5 Relationship between noise and size of B_S.

of moonlight and background noise, $N(x,y) > K(x,y)$ exists.

Third, $K(x,y)$ subtracts the minimum of $K(x,y)$ and $N(x,y)$ to obtain $R(x,y)$. In the regions of noise and moonlight where $N(x,y) > K(x,y)$, $R(x,y) = 0$, the interferences are suppressed; in the star region where $N(x,y) < K(x,y)$, $R(x,y) > 0$, if $R(x,y) > 0$, then the pixel of (x,y) in the image is considered a star pixel, so star segmentation is realized. Subsequently, the star region is segmented, as shown by the yellow region in Fig. 4(a), and moonlight interference and background noise are suppressed.

3 Influence of the Size of Structuring Elements

NSTS utilizes a combination of three different structuring elements; therefore, it has several properties.

3.1 *Relationship Between Noise and Size of B_S*

The opening operation can remove the bright region whose size is smaller than that of a structuring element. Thus, different structuring elements B_S can remove different sizes of noise in a star image. The structuring element B_S is accordingly selected on the basis of the size features of noise, as shown in Fig. 5.

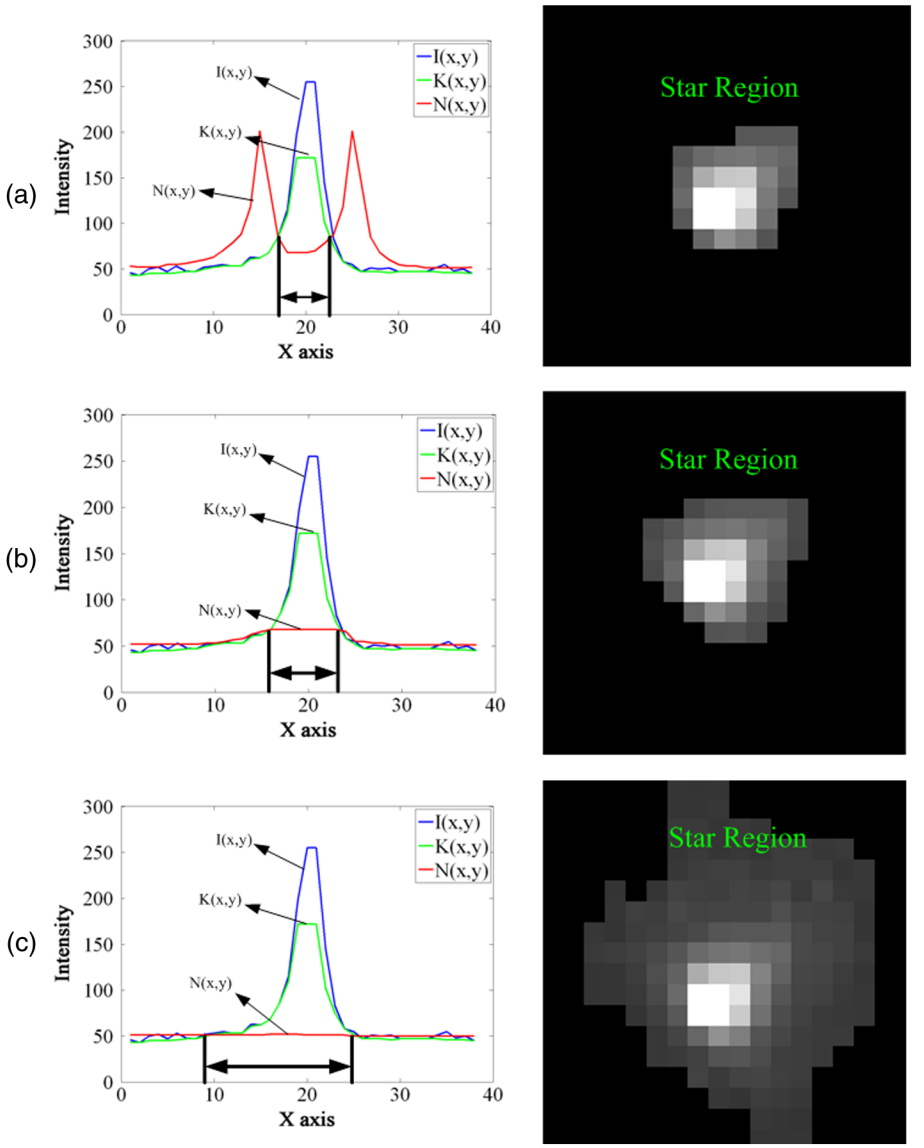

Fig. 6 Segmentation result of different $D(B_E)$.

3.2 *Relationship Between $D(B_E)$ and the Integrity of Star Segmentation*

The definitions of dilation and erosion indicate that dilation increases the size of the bright regions of an image and decreases the size of the dark regions of an image. Erosion decreases the size of bright regions and increases the size of dark regions. The influence of $D(B_E)$ on star segmentation is shown in Fig. 6.

If $D(B_E) < D(B_{Mo})$, then the bright regions of an image decrease significantly. As a result, the star region becomes small, thereby affecting star centroiding accuracy, as shown in Fig. 6(a). If $D(B_E) = D(B_{Mo})$, then the bright regions of an image and the size of the star region do not change. Hence, the segmented star is complete, which facilitates high star centroiding accuracy, as shown in Fig. 6(b). If $D(B_E) > D(B_{Mo})$, then the bright regions of an image increase significantly. The star region becomes large, and the surrounding noise can be segmented. The noise suppression capability is weakened consequently, as shown in Fig. 6(c).

Figure 6 shows that different $D(B_E)$ values influence the integrity of star segmentation but can still be used to segment stars. Therefore, the number of segmented stars is unaffected.

3.3 *Relationship Between $D(B_{Mi})$ and Star Size*

Because the size of structuring elements influences the noise suppressing capability and the result of star segmentation, to segment stars completely, $D(B_{Mi})$ should be larger than the size of stars; otherwise, only a part of the star area can be segmented on the basis of the definition of dilation and the characteristics of the margin structuring element. This condition in turn reduces star centroiding accuracy, as shown in Fig. 7.

3.4 *Relationship Between $D(B_{Mi})$ and the Number of Segmented Stars*

To determine the value of $D(B_{Mi})$, $D(B_{Mi})$ is changed, the width of B_M is fixed as 1, 100 star images with different attitude angles are simulated, Gaussian noise is added, and the average number of segmented stars after processing with different $D(B_{Mi})$ is calculated. As shown in Fig. 8, with increasing $D(B_{Mi})$, if $D(B_{Mi}) < 9$, then the number of segmented stars increases; if $D(B_{Mi}) > 9$, then the number of segmented stars has no significant change and thus $D(B_{Mi}) = 9$.

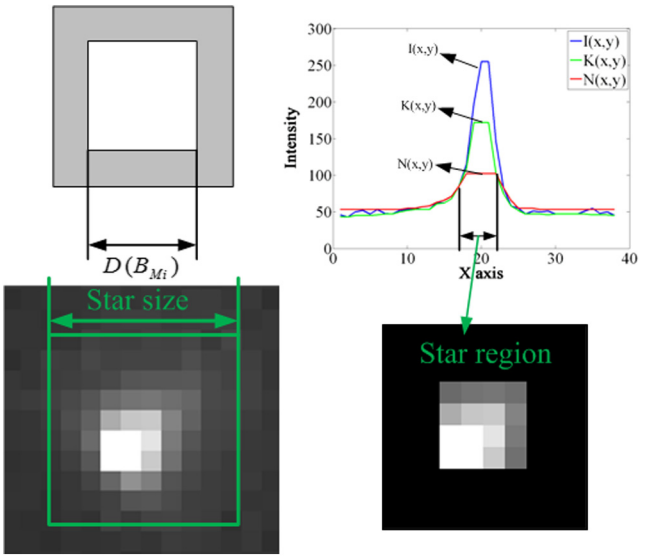

Fig. 7 Segmentation result with $D(B_{Mi})$ smaller than the star.

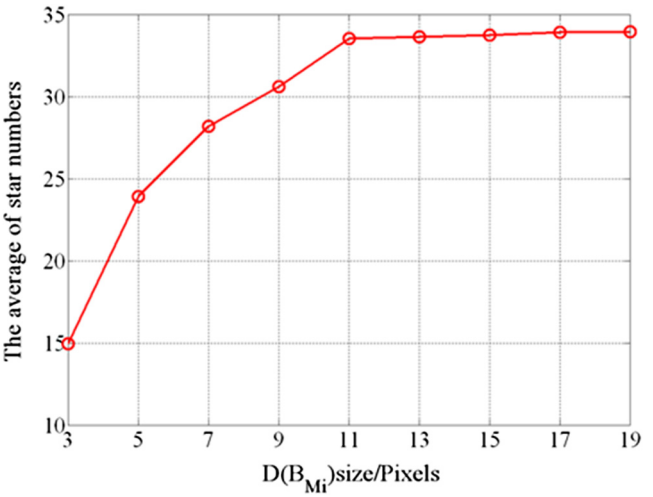

Fig. 8 Relationship between $D(B_{Mi})$ and number of segmented stars.

3.5 *Relationship Between $d(B_M)$ and the Number of Segmented Stars*

The definition of NWTH indicates that a large $D(B_{Mo})$ results in a large region in the margin structuring element and strong noise smoothing capability. Nevertheless, dim stars are removed, thereby reducing the number of segmented stars and influencing star identification. NSTS relies on the size of B_S to suppress noise. Therefore, even if the width of the margin structuring element is small, the noise suppression capability of NSTS is not influenced. To determine the value of $d(B_M)$, $D(B_{Mi})$ is fixed as 9, $d(B_M)$ is changed, 100 star images with different attitude angles are simulated, Gaussian noise is added, and the average number of segmented stars after processing with different $d(B_M)$ is calculated. As shown in Fig. 9, the number of segmented stars decreases with increasing $d(B_M)$; thus, $d(B_M) = 1$ and $D(B_{Mo}) = 11$.

4 Experiments and Results

Several experiments were conducted for simulated and real star images on software platforms to verify the superiority of NSTS. In these experiments, based on the analysis of the size of structuring elements in Sec. 3, we set $D(B_{Mi}) = 9$, $D(B_{Mo}) = 11$, $d(B_M) = 1$, and $D(B_E) = 11$. B_S is denoted as a square structuring element with a size of 3×3 pixels.

4.1 *Capability to Suppress Different Interferences*

Arbabmir's algorithms, NWTH, and Mao's algorithm were applied to several star images with different interferences to demonstrate the performance of NSTS in suppressing different interferences. These methods were used for comparison with NSTS. Figure 10(a) shows the original star image with different interferences; from top to bottom are star images with noise, ghost noise, and moonlight. Figure 10(b) shows

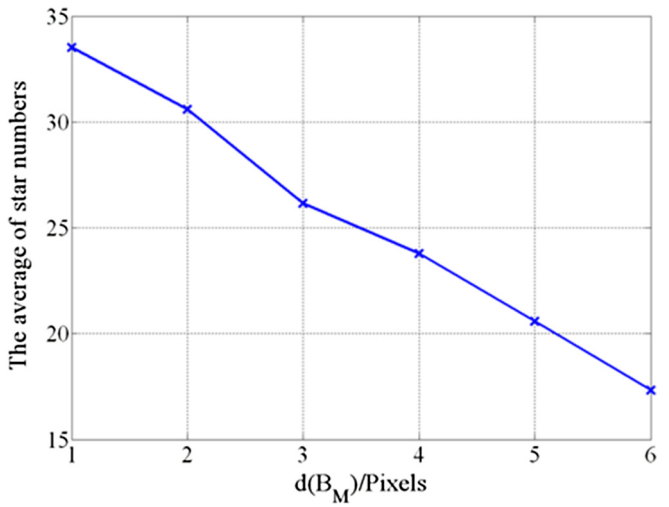

Fig. 9 Relationship between $d(B_M)$ and number of segmented stars.

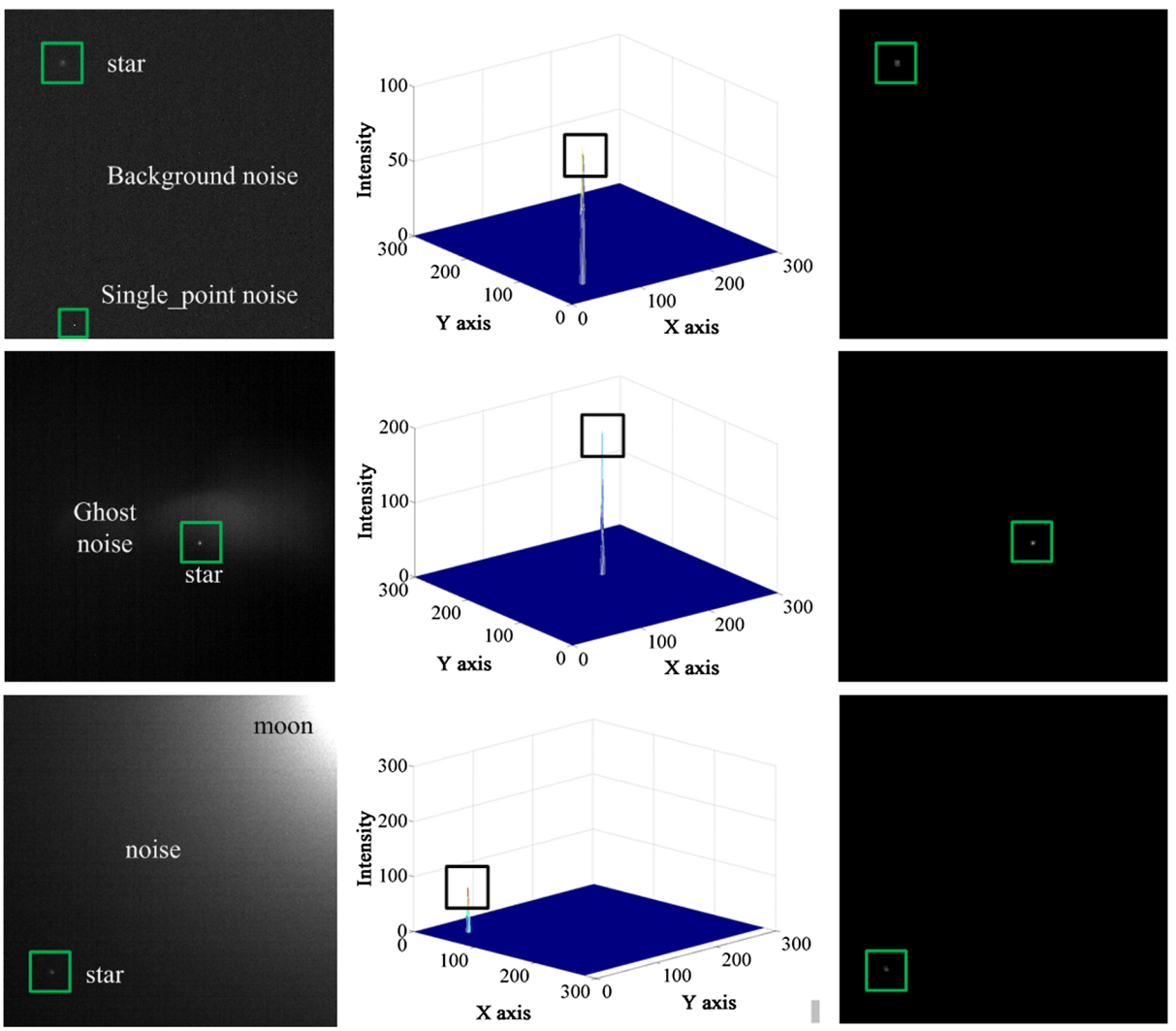

Fig. 10 Star image with different interferences and segmentation result by using NSTS: (a) original star image with different interferences, (b) 3-D distribution of the segmentation result by using NSTS, and (c) segmentation result by using NSTS.

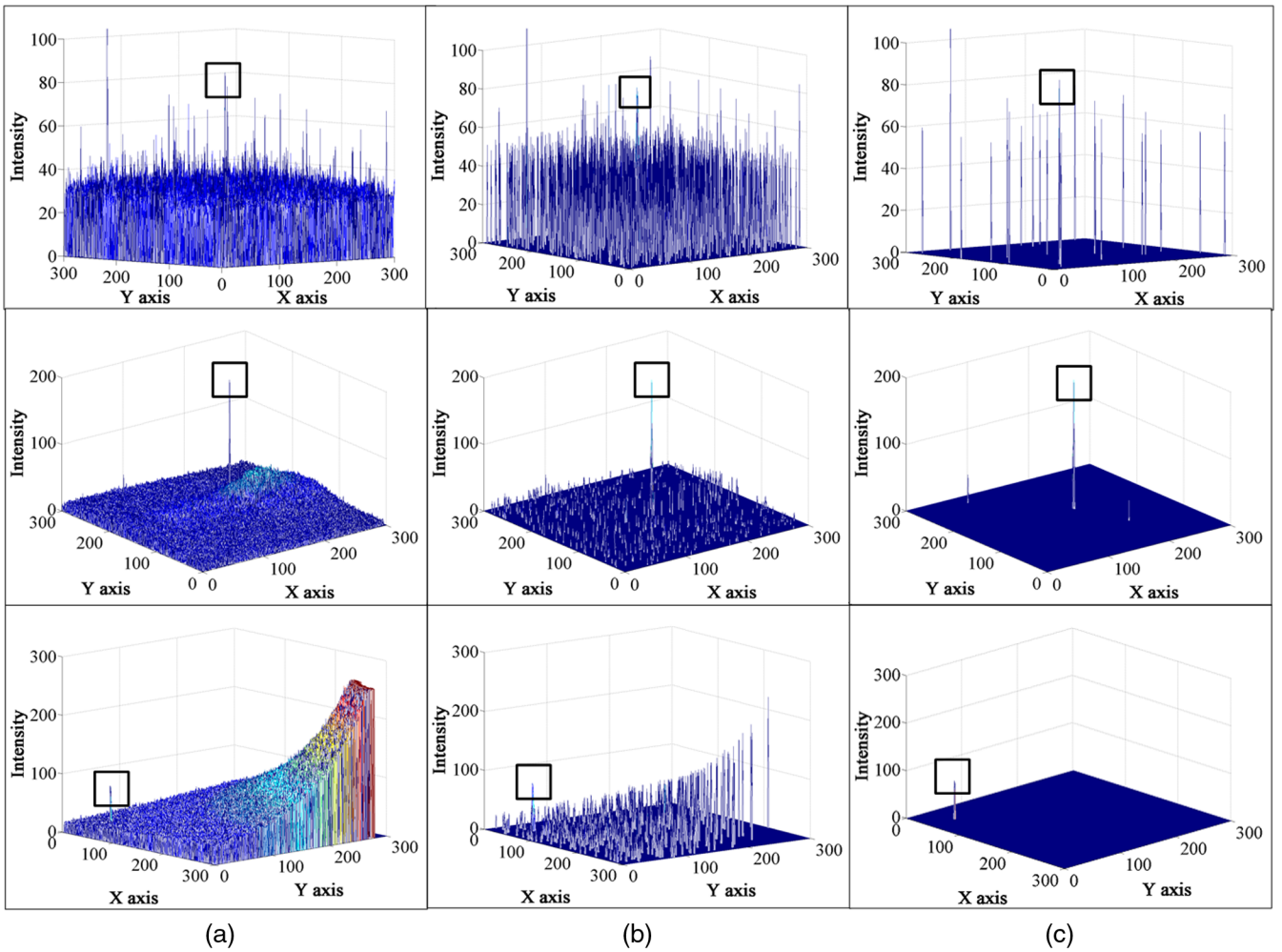

Fig. 11 Segmentation result of other algorithms: (a) Arbabmir's algorithm, (b) NWTH, and (c) Mao's algorithm.

the three-dimensional (3-D) distribution of the segmentation result using NSTS. Figure 10(c) shows the segmentation result using NSTS. The experimental results demonstrate that NSTS can suppress different interferences and segment stars at the same time.

Figure 11(a) shows the 3-D distribution of the segmentation result using Arbabmir's algorithm. Figure 11(b) shows the 3-D distribution of the segmentation result using NWTH, and Fig. 11(c) shows the 3-D distribution of the segmentation result using Mao's algorithm. The results show that Arbabmir's algorithm cannot suppress interference effectively. NWTH suppresses interference to some extent, but still cannot suppress the single-point noise. Mao's algorithm suppresses most interference, but it cannot suppress a single-point noise with high gray.

4.2 *Integrity of Star Segmentation and Accuracy of Star Centroid*

4.2.1 *Integrity of star segmentation*

Arbabmir's algorithm, Mao's algorithm, and NSTS were utilized to segment the real star image to verify the capability for accurate star segmentation. In Fig. 12, (a) is the original star with different magnitude, (b) is the segmentation result with NSTS, (c) is the segmentation result with Mao's algorithm, and (d) is the segmentation result with Arbabmir's algorithm. Only the relatively high gray pixel in the star can be segmented by Arbabmir's and Mao's algorithms. By contrast, NSTS segments stars completely, which improves the star centroiding accuracy.

4.2.2 *Accuracy of star segmentation*

Several simulated star images with different Gaussian noises were generated to verify the segmentation accuracy for star segmentation. A star image with four magnitudes was simulated. Gaussian noise with σ_n from 0.001 to 0.01 was added. The proposed algorithm along with Mao's and Arbabmir's algorithms were then used to segment stars. The traditional square weighted centroid method was used to calculate the star centroid. The root-mean-square error of stars with different Gaussian noises is shown in Fig. 13. Mao's and Arbabmir's algorithms cannot segment the star centroid when σ_n is larger than 0.006 and 0.003, respectively. Their star centroiding accuracy is lower than that of NSTS. Given its robust noise suppression and complete star segmentation capabilities, NSTS can segment the star centroid when σ_n is high and can obtain high star centroiding accuracy with less than 0.09 pixels.

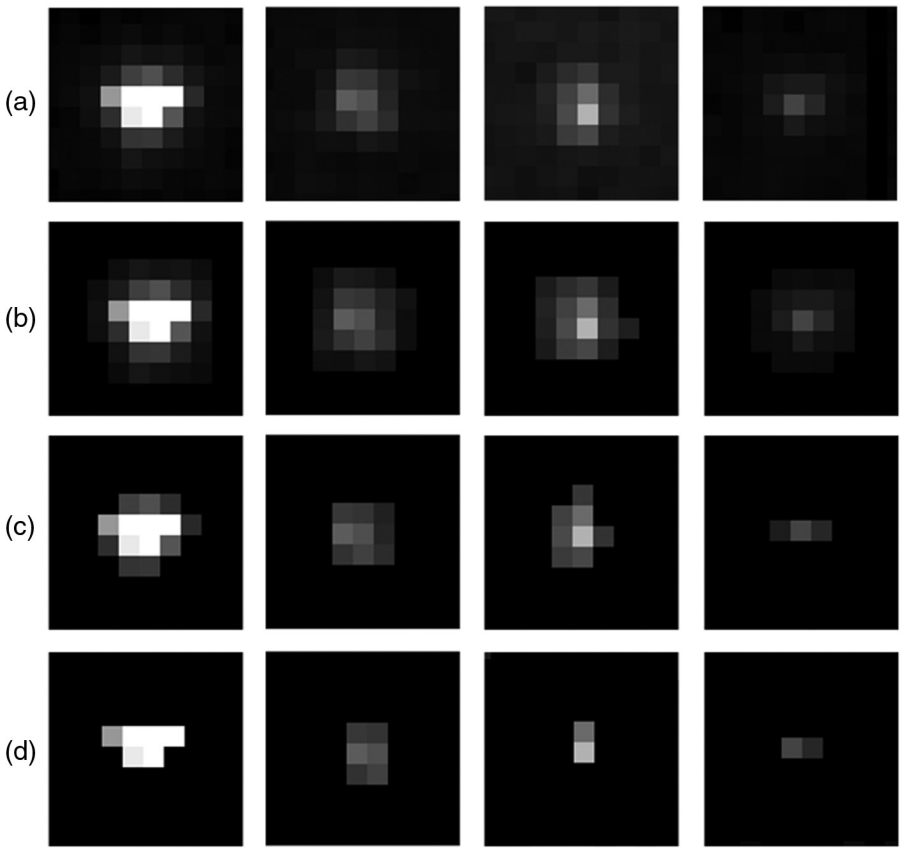

Fig. 12 Segmentation result of different magnitude star: (a) original star, (b) NSTS, (c) Mao's algorithm, and (d) Arbabmir's algorithm.

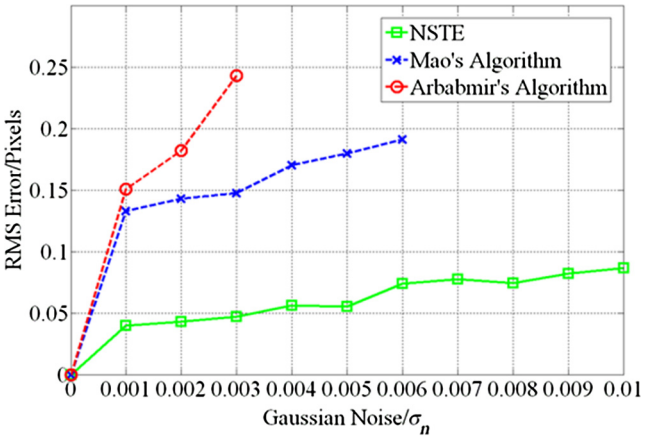

Fig. 13 Influence of Gaussian noise on the star centroid.

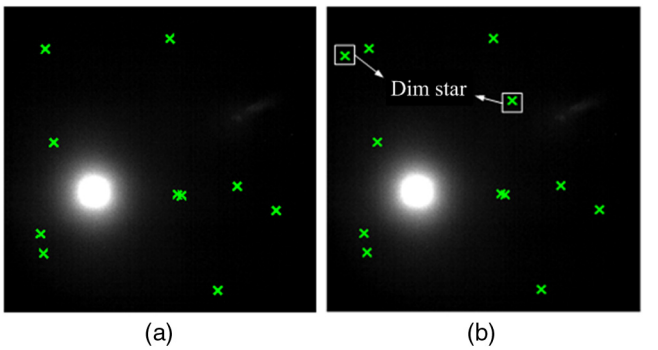

Fig. 14 Comparison of star identification result: (a) star identification result of Mao's algorithm and (b) star identification result of NSTS.

4.2.3 *Total number of segmented stars*

Mao's algorithm was compared with NSTS to validate the star segmentation performance of the latter. Given that Arbabmir's algorithm and NWTH cannot remove the interferences in a star image, star identification cannot be evaluated. After using the proposed and Mao's algorithms to segment stars, star identification[18] was performed by the same method, as shown in Fig. 14. NSTS can segment dim stars, whereas Mao's algorithm cannot. Five star images were randomly selected and processed by the two algorithms. The total number of segmented stars was calculated, as shown in Fig. 15. NSTS segments more stars effectively because of dim star segmentation; when a star image has a few stars, this property facilitates star identification.

4.2.4 *Probabilities of true detection and miss detection*

To validate probabilities of true detection and miss detection of NSTS, five star images were randomly selected and processed by the two algorithms. After using the proposed and Mao's algorithms to segment stars, star identification[21] was performed by the same method, and the probabilities of true

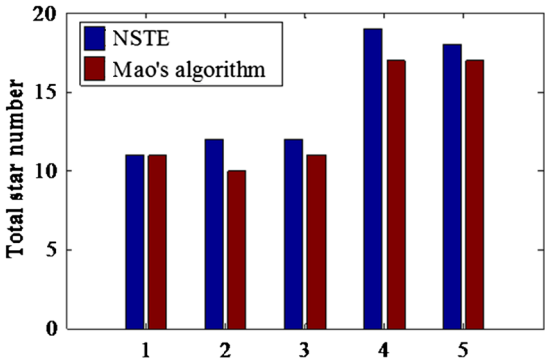

Fig. 15 Comparison of the total number of identified stars.

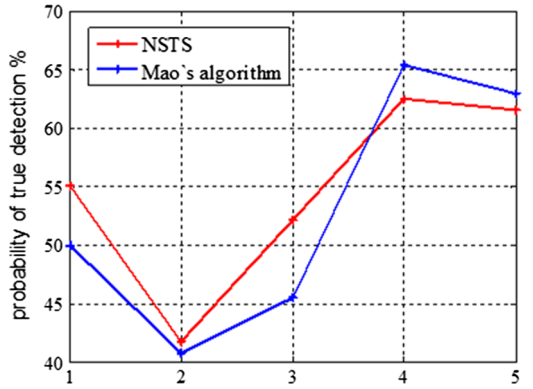

Fig. 16 Comparison of the probability of true detection.

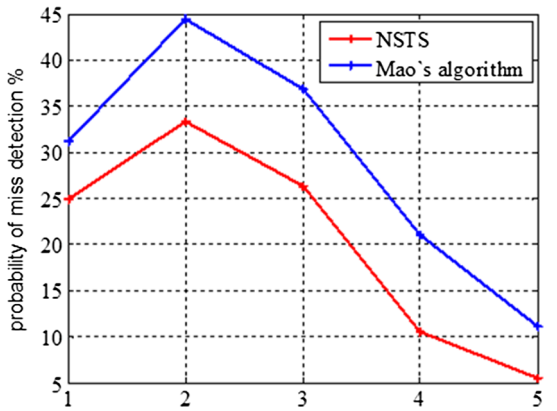

Fig. 17 Comparison of the probability of miss detection.

detection and miss detection were calculated. As shown in Figs. 16 and 17, the probability of true detection of two algorithms does not differ greatly from each other. However, NSTS can segment more potential stars than Mao's algorithm; as a result the probability of miss detection for NSTS is lower than Mao's algorithm.

4.3 *Comparison of Computation Time*

In Table 1, the computation time for all algorithms applied to a given 1024×1024 test image is shown. All images and algorithms were simulated in MATLAB® (R2010a) in a PC with a 2.93-GHz Core 2 Duo CPU, 2.00 GB RAM, and a Window's XP operational system. The results show that NSTS is faster than NWTH and Arbabmir's algorithm, which result from the decrease in the size of the margin structuring element, thereby reducing the amount of calculation and increasing the computational speed. NSTS is slower than Mao's algorithm; the computation of the latter is simple, but its star segmentation is incomplete.

Table 1 Computation time of four approaches applied to a 1024×1024 star image.

Segmentation approaches	Computation times (s)
Mao's algorithm	0.2344
Arbabmir's algorithm	0.3515
NWTH	0.6526
NSTS	0.3299

5 Conclusion and Discussion

The current star segmentation algorithm cannot suppress different interferences in star images and cannot segment stars completely because of these interferences. To overcome this problem, a combination of three different structuring elements is used to define a new star segmentation algorithm. By considering star image characteristics with different interferences, the proposed algorithm utilizes the margin structuring element to detect small targets and opening operation to suppress noises, and a modified top-hat transform is defined to extract stars. Compared with the current star segmentation algorithm, the experimental results show that NSTS has good robustness against different interferences and both bright stars and dim stars can be segmented completely by the proposed algorithm. These results also show that a precision of less than 0.09 pixels can be maintained under different levels of noise by the proposed algorithm with the traditional square weighted centroid method. Therefore, NSTS is reasonable and effective to use for accurate star segmentation with different interferences. Because mathematical morphology is based on window operation, we plan to implement the proposed algorithm to FPGA in further work.

Acknowledgments

This research was supported by the National Natural Science Fund of China under Grant No. 61222304 and grants from the Specialized Research Fund for the Doctoral Program of Higher Education of China (No. 20121102110032). The authors are grateful for all the valuable suggestions received during the course of this work.

References

1. B. R. Hancock, R. C. Stirbi, and T. J. Cunningham, "CMOS active pixel sensor specific performance effects on star tracker/imager position accuracy," *Proc. SPIE* **4284**, 43 (2001).
2. M. V. Arbabmir et al., "Improving night sky star image processing algorithm for star sensors," *JOSA A* **31**(4), 794–801 (2014).
3. C. C. Liebe, "Accuracy performance of star trackers-a tutorial," *IEEE Trans. Aerosp. Electron. Syst.* **38**, 587–599 (2002).
4. X. Wei et al., "Exposure time optimization for highly dynamic star trackers," *Sensors* **14**(3), 4914–4931 (2014).
5. C. C. Liebe, "Star trackers for attitude determination," *IEEE Aerosp. Electron. Syst. Mag.* **10**(6), 10–16 (1995).

6. M. Sezgin, "Survey over image thresholding techniques and quantitative performance evaluation," *J. Electron. Imaging* **13**(1), 146–168 (2004).
7. W. Xu, Q. Li, and H.-J. Feng, "A novel star image thresholding method for effective segmentation and centroid statistics," *Optik* **124**, 4673–4677 (2013).
8. W. Xu, Q. Li, and H. Feng, "A novel star image thresholding method for effective segmentation and centroid statistics," *Optik* **124**(20), 4673–4677 (2013).
9. J.-L. Fan and B. Lei, "A modified valley-emphasis method for automatic thresholding," *Pattern Recognit. Lett.* **33**, 703–708 (2012).
10. X. N. Mao, W. S. Liang, and X. J. Zheng, "A parallel computing architecture based image processing algorithm for star sensor," *J. Astronaut.* **32**(3), 613–619 (2011). (in Chinese)
11. J. Han, Y. Ma, and B. Zhou, "A robust infrared small target detection algorithm based on human visual system," *IEEE Geosci. Remote Sens. Lett.* **11**(12), 2168–2172 (2014).
12. S. Kim and J. Lee, "Scale invariant small target detection by optimizing signal-to-clutter ratio in heterogeneous background for infrared search and track," *Pattern Recognit.* **45**(1), 393–406 (2012).
13. T. Bae, "Small target detection using bilateral filter and temporal cross product in infrared images," *Infrared Phys. Technol.* **54**(5), 403–411 (2011).
14. Y. Cao, R. Liu, and J. Yang, "Small target detection using two-dimensional least mean square (TDLMS) filter based on neighborhood analysis," *Int. J. Infrared Millimeter Waves* **29**(2), 188–200 (2008).
15. F. Zhang, C. Li, and L. Shi, "Detecting and tracking dim moving point target in IR image sequences," *Infrared Phys. Technol.* **46**, 323–328 (2005).
16. B. Ye and J. Peng, "Small target detection method based on morphology top-hat operator," *J. Image Graph.* **7**(7), 638–642 (2002).
17. M. Zeng, J. Li, and Z. Peng, "The design of top-hat morphological filter and application to infrared target detection," *Infrared Phys. Technol.* **48**, 1350–4495 (2006).
18. P. T. Jackway, "Improved morphological top-hat," *Electron. Lett.* **36**(14), 1194–1195 (2000).
19. X. Bai and F. Zhou, "Analysis of new top-hat transformation and the application for infrared dim small target detection," *Pattern Recognit.* **43**(6), 2145–2156 (2011).
20. J. Serra, *Image Analysis and Mathematical Morphology*, Academic Press, New York (1982).
21. J. Jiang, F. Ji, and J. Yan, "Redundant-coded radial and neighbor star pattern identification algorithm," *IEEE Trans. Aerosp. Electron. Syst.* **51**(4), 2811–2822 (2015).

Jie Jiang is currently a professor of the School of Instrumentation Science and Opto-Electronics Engineering, Beihang University (BUAA), China. She received her bachelor's, master's, and PhD degrees from Tianjing University from 1991 to 2000. Her research interests include image processing and precision measurement.

Lei Liu received his bachelor's and master's degrees in instrument science and technology in 2014 from the University of Science and Technology Beijing (USTB), China. Since 2014, he has been pursuing a doctoral degree in the Department of Instrumentation Science and Opto-Electronics Engineering, Beihang University (BUAA), China. His current interests include precision measurement and image processing.

Guangjun Zhang received his PhD from the Department of Precision Instrumentation Engineering of Tianjin University, China, in 1991. He was a visiting professor at North Dakota State University from 1997 to 1998. He was a Yangtze River Scholar Award Program Professor in 2000. Currently, he is a professor in the School of Instrumentation Science and Opto-Electronics Engineering, Beihang University, China. His research interests are laser precision measurement, machine vision, and optical sensing.